Journal of Pathology
J Pathol (2009)
Published online in Wiley InterScience
(www.interscience.wiley.com) **DOI:** 10.1002/path.2591

Original Paper

Up-regulation of autophagy in small intestine Paneth cells in response to total-body γ-irradiation††

Nikolai V. Gorbunov[1†*] and Juliann G. Kiang[1,2†*]

[1] *Radiation Combined Injury Program, Armed Forces Radiobiology Research Institute (AFRRI), Bethesda, MD 20889-5603, USA*
[2] *Department of Radiation Biology and of Medicine, Uniformed Services University of the Health Sciences, Bethesda, MD 20889-5603, USA*

**Correspondence to:*
Juliann G. Kiang, Armed Forces Radiobiology Research Institute, 8901 Wisconsin Avenue, Bethesda, MD 20889-5603, USA.
E-mail: kiang@afrri.usuhs.mil

Dr Nikolai V. Gorbunov, Armed Forces Radiobiology Research Institute, 8901 Wisconsin Avenue, Bethesda, MD 20889-5603.
E-mail: gorbunov@afrri.usuhs.mil

†*Both authors contributed equally to the presented work.*

††*The opinions or assertions contained herein are the authors' private views and are not to be construed as official or reflecting the views of the Uniformed Services University of the Health Sciences or the US Department of defence.*

No conflicts of interest were declared.

Received: 6 January 2009
Revised: 18 May 2009
Accepted: 8 June 2009

Abstract

Macroautophagy (mAG) is a lysosomal mechanism of degradation of cell self-constituents damaged due to variety of stress factors, including ionizing irradiation. Activation of mAG requires expression of mAG protein Atg8 (LC3) and conversion of its form I (LC3-I) to form II (LC3-II), mediated by redox-sensitive Atg4 protease. We have demonstrated upregulation of this pathway in the innate host defense Paneth cells of the small intestine (SI) due to ionizing irradiation and correlation of this effect with induction of pro-oxidant inducible nitric oxide synthase (iNOS). CD2F1 mice were exposed to 9.25 Gy γ-ionizing irradiation. Small intestinal specimens were collected during 7 days after ionizing irradiation. Assessment of ionizing irradiation-associated alterations in small intestinal crypt and villus cells and activation of the mAG pathway was conducted using microscopical and biochemical techniques. Analysis of iNOS protein and the associated formation of nitrites and lipid peroxidation products was performed using immunoblotting and biochemical analysis, and revealed increases in iNOS protein, nitrate levels and oxidative stress at day 1 following ionizing irradiation. Increase in immunoreactivity of LC3 protein in the crypt cells was observed at day 7 following ionizing irradiation. This effect predominantly occurred in the CD15-positive Paneth cells and was associated with accumulation of LC3-II isoform. The formation of autophagosomes in Paneth cells was confirmed by transmission electron microscopy (TEM). Up-regulation of LC3 pathway in the irradiated SI was accompanied by a decreased protein–protein interaction between LC3 and chaperone heat shock protein 70. A high-level of LC3-immunoreactivity in vacuole-shaped structures was spatially co-localized with immunoreactivity of 3-nitro-tyrosine. The observed effects were diminished in iNOS knockout B6.129P2-*NOS2*^{tm1Lau}/J mice subjected to the same treatments. We postulate that the observed up-regulation of mAG in the irradiated small intestine is at least in part mediated by the iNOS signalling mechanism.
Published in 2009 by John Wiley & Sons, Ltd.

Keywords: LC3 protein; autophagy; Paneth cells; ionizing irradiation; iNOS; nitration; oxidative stress

Introduction

Irradiation remains a major therapy for cancer treatment [1,2]. The total delivered radiation dose is limited because effect of ionizing irradiation in normal tissues can cause damage to their barrier functions, resulting in systemic failure, [1–3]. The role of macroautophagy (mAG) in the molecular mechanisms of ionizing radiation-induced response in normal cells, especially in the cells of dose-sensitive tissues such as small intestine, is not clear. Of particular interest is whether mAG contributes to the ionizing irradiation response in small intestinal host-defence cells such as Paneth cells, which are considered to be relatively resistant to ionizing irradiation and therefore can maintain barrier homeostasis after lethal ionizing irradiation exposure [4–8].

mAG is responsible for the routine bulk degradation of redundant or defective organelles, long-lived proteins, large macromolecules and pathogens, and thus provides a homeostatic balance of biosynthetic and biodegradative activities and innate immunity [9–12]. mAG is characterized by the formation of autophagosomes, where portions of the cytoplasm are sequestered, cargo-packaged within a double membrane-enclosed vacuole and transported to lysosomes or late endosomes for biodegradation [11–14]. A key step in this process is the conversion of light-chain protein 3 type I (LC3-I; also known as ubiqitin-like protein, Atg8) to type II (LC3-II). The conversion occurs via the cleavage of the LC3-I carboxyl terminus by a redox-sensitive Atg4 cysteine protease. The subsequent binding of the modified LC3-I to

Report Documentation Page

Form Approved
OMB No. 0704-0188

1. REPORT DATE	2. REPORT TYPE	3. DATES COVERED
2009		**00-00-2009 to 00-00-2009**

4. TITLE AND SUBTITLE	5a. CONTRACT NUMBER
Up-regulation of autophagy in small intestine Paneth cells in response to total-body γ -irradiation	5b. GRANT NUMBER
	5c. PROGRAM ELEMENT NUMBER
6. AUTHOR(S)	5d. PROJECT NUMBER
	5e. TASK NUMBER
	5f. WORK UNIT NUMBER
7. PERFORMING ORGANIZATION NAME(S) AND ADDRESS(ES) **Radiation Combined Injury Program,Armed Forces Radiobiology Research Institute (AFRRI),Bethesda,MD,20889-5063**	8. PERFORMING ORGANIZATION REPORT NUMBER
9. SPONSORING/MONITORING AGENCY NAME(S) AND ADDRESS(ES)	10. SPONSOR/MONITOR'S ACRONYM(S)
	11. SPONSOR/MONITOR'S REPORT NUMBER(S)

12. DISTRIBUTION/AVAILABILITY STATEMENT
Approved for public release; distribution unlimited

13. SUPPLEMENTARY NOTES

14. ABSTRACT

15. SUBJECT TERMS

16. SECURITY CLASSIFICATION OF:			17. LIMITATION OF ABSTRACT	18. NUMBER OF PAGES	19a. NAME OF RESPONSIBLE PERSON
a. REPORT	b. ABSTRACT	c. THIS PAGE			
unclassified	**unclassified**	**unclassified**	**Same as Report (SAR)**	**11**	

phosphatidylethanolamine on the forming isolation membrane is mediated by E-1- and E-2-like enzymes Atg7 and Atg3 [15–17]. Therefore, LC3-II protein is considered to be a marker of an autophagosome [16,17]. In addition to normal homeostatic function, mAG is induced in response to certain conditions, including ionizing irradiation [11,12,18–20]. Induction of mAG in response to redox stress can be either protective or detrimental when it results from massive free radical oxidative damage to biomolecules and organelles [20–22]. Although the free radical species produced by ionizing irradiation have a short-term effect, the radiation-induced activation of pro-oxidant pathways, such as a signaling pathway of the inducible nitric oxide synthase (iNOS), can potentiate and prolong oxidation and thus can extend up-regulation of mAG.

To address ionizing irradiation effects on mAG in Paneth cells, we used CD2F1 mice exposed to 9.25 Gy γ-ionizing irradiation and conducted assessment of biochemical and morphological alterations at various days post-exposure. Analysis of small intestinal specimens revealed an increase in iNOS protein, NO, oxidative stress and protein nitration that was accompanied by dramatic increase in immunoreactivity for the LC3-II isoform, which was predominantly observed in CD15-positive crypt Paneth cells. This increase was associated with the formation of distinguishable LC3-positive vacuoles identified, using transmission electron microscopy (TEM), as autophagosomes. A high level of LC3-immunoreactivity in vacuole-shaped structures was spatially co-localized with immunoreactivity of 3-nitrotyrosine (3NTyr). The observed effects were diminished in iNOS knockout B6.129P2-*NOS2*^{tm1Lau}/J mice subjected to the same treatments. Therefore, the results suggest that the iNOS signalling mechanism can partially contribute to the observed activation of mAG in the irradiated small intestine.

Materials and methods

Animals

CD2F1 and B6.129P2-*NOS2*^{tm1Lau}/J male mice were purchased from Harlan Laboratories (Indianpolis, IN, USA) and Jackson Laboratories (Bar Harbor, ME, USA), respectively. Thirty randomly selected mice, 25 g in weight, were assigned to five experimental groups, placed in acrylic Plexiglas restrainers and given 9.25 Gy total-body ^{60}Co γ-photon radiation at 0.6 Gy/min in the AFRRI radiation facility. Fifteen additional mice were assigned to five sham groups and subjected to all the above treatments except irradiation. Irradiated and sham-treated animals were euthanized at days 1, 2, 3, 5 and 7 post-treatment. Small intestinal specimens were harvested and kept frozen at $-80\,^{\circ}$C until analysed. Research was conducted in a facility accredited by the Association for the Assessment and Accreditation of Laboratory Animal Care — International (AAALAC–I). All animals used in this study received humane care in compliance with the Animal Welfare Act and other federal statutes and regulations relating to animals and experiments involving animals, and adhered to principles stated in the *Guide for the Care and Use of Laboratory Animals* [23].

Histology and TUNEL staining for assessment of apoptosis

Small intestinal specimens were fixed in 10% buffered formalin, embedded in paraffin and subjected to sectioning. The sections were stained with haematoxylin and eosin for histological examination. Crypts and Paneth cells were identified according to the criteria established by Withers and Elkind [24], Hampton [8], Garabedian *et al* [25], Potten *et al* [26] and Barker *et al* [27]. Terminal deoxynucleotidyl transferase biotin–dUTP nick end labelling (TUNEL) staining for apoptosis was conducted with a provision of the manufacturer's recommendations (Upstate/Millipore; www.millipore.com).

Immunoblotting

To analyze iNOS, BAG-1, LC3-I, LC3-II, "α-defensin-4 and IgG, small intestinal tissues were minced and sonicated in 200 µl sodium Hanks' solution (SHS) containing protease inhibitors.The total protein in the tissue lysate was determined with Bio-Rad reagent 500-0002 (Bio-Rad, Richmond, CA, USA). Aliquots containing 20 µg protein in Tris buffer, pH = 6.8, containing 1% sodium dodecyl sulphate (SDS) and 1% 2-mercaptoethanol were resolved on SDS–polyacrylamide slab gels (NuPAGE 4–12% Bis-Tris; Invitrogen, Carlsbad, CA, USA). After electrophoresis, proteins were blotted onto a PVDF nitrocellulose membrane (0.45 µm; Invitrogen, cat. # LC2005). The blots were incubated with monoclonal antibodies (1 µg/ml) raised against MAP LC3, BAG-1, iNOS (Santa Cruz Biotechnology, BD Signal Transduction, KY, USA), followed by incubation with species-specific IgG peroxidase conjugate. The peroxidase activity was determined using the Enhanced Chemiluminenscence Plus (Amersham Life Science, Arlington Heights, IL, USA). IgG levels were not altered by radiation; we therefore used IgG as a control for protein loading. Protein bands of interest were quantitated densitometrically and normalized to IgG.

Immunoprecipitation

Tissue lysates containing 300 µg protein were incubated with antibodies for heat shock protein 70 kDa (HSP-70, 5 µl; Santa Cruz Biotechnology, CA, USA), chilled on ice for 1 h, mixed with protein A/G agarose beads (50 µl; Santa Cruz Biotechnology), and incubated overnight on a nutator at 4 °C. The immunoprecipitate was collected by centrifugation at

12 500 × g for 10 min, washed twice with 500 μl SHS stop buffer and once with 500 μl SHS wash buffer. The pellet was resuspended in 50 μl electrophoresis sample buffer, boiled for 5 min and then centrifuged for 30 s to remove the agarose beads. The supernatant was incubated with 5% 2-mercaptoethanol at 37 °C for 1 h and then analysed with immunoblotting, as described above.

Nitric oxide and lipid peroxidation (LPO) measurements

NO production was measured under acidic conditions as nitrite, using the Griess Reagent System with sulphanilamide and *N*-1-napthylethylenediamine dihydrochloride (Promega, Madison, WI, USA). Malondialdehyde (MDA), a lipid peroxidation end-product, was measured colorimetrically using a commercial assay kit (CalBiochem, San Diego, CA, USA).

Transmission electron microscopy (TEM)

Slices (2−3 mm) of tissue were fixed in 4% formaldehyde and 4% glutaraldehyde in PBS overnight, post-fixed in 2% osmium tetroxide in PBS, dehydrated in a graduated series of ethanol and embedded in Spurr's epoxy resin. Blocks were cut on a Leica Ultracut ultramicrotome. Sections 1 μm thick were stained with toluidine blue and examined by light microscopy. Thin (80 nm) sections were stained with 2% uranyl acetate and Reynolds' lead citrate for TEM, which was performed on a Philips CM100 electron microscope.

Immunofluorescence staining

The cryotomy, immunostaining and confocal image analysis of small intestine specimens were conducted as described previously [28,29]. The primary antibodies were against: (a) MAP LC3 (goat polyclonal IgG; Santa Cruz Biotechnology); (b) CD-15 (biotin-labeled mouse polyclonal IgM; eBioscience); (c) anti-3-nitrotyrosine (rabbit IgG from Upstate/Millipore; www.upstate.com). This was followed by incubation with secondary fluorochrome-conjugated antibody and/or streptavidin-AlexaFluor 610 conjugate (Molecular Probes) and with Hoechst 33 342 for counterstaining of the nuclei. The secondary antibodies used were: (i) ALEXA 488-conjugated donkey anti-goat IgG (Molecular Probes); (ii) ALEXA 594-conjugated donkey anti-rabbit IgG (Molecular Probes). Negative controls for non-specific binding included normal donkey serum without primary antibody or with secondary antibody alone. The specificity of binding of anti-3-nitrotyrosine antibody was tested as described previously [29].

Statistical analysis

The values for immunochemical and biochemical data are all expressed as the mean ± standard error of the mean (SEM). Analysis of variance procedures with Tukey *post hoc* correction examined the existence and nature of temporal trends among the treatment (viz. sampling time periods post-exposure) level means. Student's *t*-test was also performed. Results were considered significant when $p < 0.05$.

Solutions

Sodium Hanks' solution (SHS) contained in mM: 145 NaCl, 4.5 KCl, 1.3 $MgCl_2$, 1.6 $CaCl_2$, and 10 HEPES (pH 7.40 at 24 °C). The protease inhibitors in HSS included 1 mM EDTA, 1 mM phenylmethanesulfonyl fluoride, 1 mM DTT, 1 mM Na_3VO_4, 1 mM NaF, along with aprotinin, leupeptin, and pepstatin (10 μg/ml each). SHS stop buffer contained 50 mM tris-HCl, 1% NP-40, 0.25% Na^+-deoxycholate, 150 mM NaCl, 1 mM EDTA, 1 mM phenylmethanesulfonyl fluoride, 1 mM Na_3VO_4, 1 mM NaF, along with aprotinin, leupeptin, and pepstatin (10 μg/ml each). SHS wash buffer contained 1 mM EDTA, 1 mM phenylmethanesulfonyl fluoride, 1 mM DTT, 1 mM Na_3VO_4, 1 mM NaF, along with aprotinin, leupeptin, and pepstatin (10 μg/ml each).

Results

Up-regulation of autophagy in small intestine of irradiated mice

Exposure of CD2F1 mice to 9.25 Gy γ-ionizing irradiation (^{60}Co) induced animal death at day 15 post-exposure (mortality rate, 85−100%). During the first 7 days post-ionizing irradiation, there were no documented crypt denudations or morphological changes (Figure 1), except for the appearance of apoptotic transformations at the top of villi (Figure 2). As shown in Figure 3A, a substantial increase in LC3-II isoform was observed in western blots of small intestine tissue at day 7 post-exposure. We did not see alterations in the LC3-II level at day 2 following ionizing irradiation (data not shown); the elevation in the LC3-II isoform at day 3 following ionizing irradiation was not statistically significant, whereas the increase in the LC3-II levels observed at day 7 following ionizing irradiation was ∼7.5-fold higher compared to sham treatment (Figure 3A, B). Based on our observations (Figure 3A, C), the increased immunoreactivity for LC3 protein in the irradiated small intestine was predominantly due to accumulation of type II membrane-bound isoform and, thus, indicated activation of mAG pathway. Note that the balance of LC3 isoforms in irradiated lung tissue had a different pattern, as seen with the characteristic LC3-I/LC3-II double-band 'immunoprint' in the protein blotting (Figure 3C).

A growing body of evidence suggests involvement of chaperone heat shock protein 70 (HSP-70) and Bcl-2-associated athanogene-1 (*BAG-1*) in regulation of LC3-translocation. BAG-1 is a multifunctional protein, acts as a co-chaperone and exerts many of

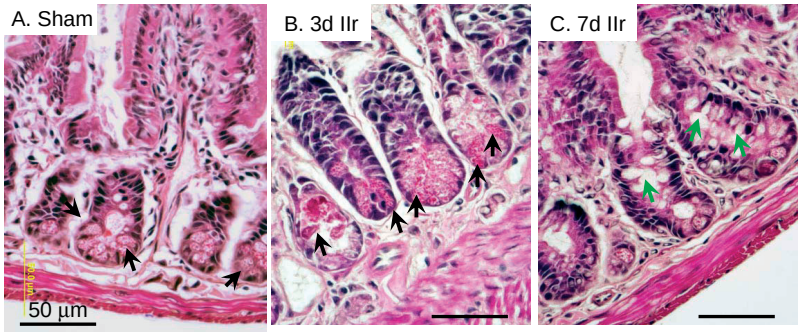

Figure 1. Histology of the small intestine crypts. (A) Specimen obtained from a sham-treated animal. (B) Specimen obtained from an irradiated animal at day 3 following ionizing irradiation (3d IIr). (C) Specimen obtained from an irradiated animal at day 7 following ionizing irradiation (7d IIr). Paneth cells are indicated by black arrows in (A, B). The Paneth cells were identified by a characteristic pyramid-like shape and abundance of granules (which appear in red). Increase in degranulation in Paneth cells was observed at day 7 following ionizing irradiation and is indicated by green arrows in (C)

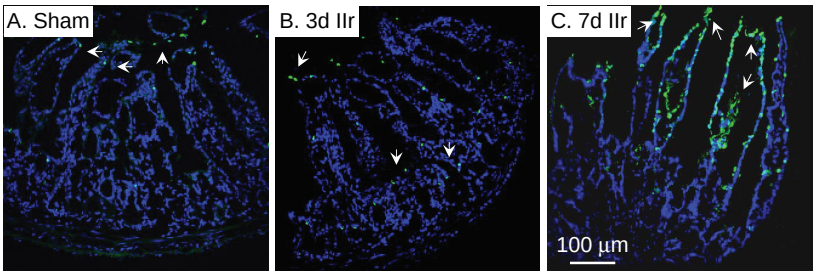

Figure 2. TUNEL assay of apoptosis in small intestine. Confocal images of apoptotic cells (green channel) were obtained from samples of sham-treated (A) and irradiated (B, C) animals. The specimens were collected at the 3rd day (B) and the 7th day (C) after irradiation. The presence of apoptotic cells (in green) is indicated by arrows. (A–C) Representative images of analyses conducted, using five specimens in each group

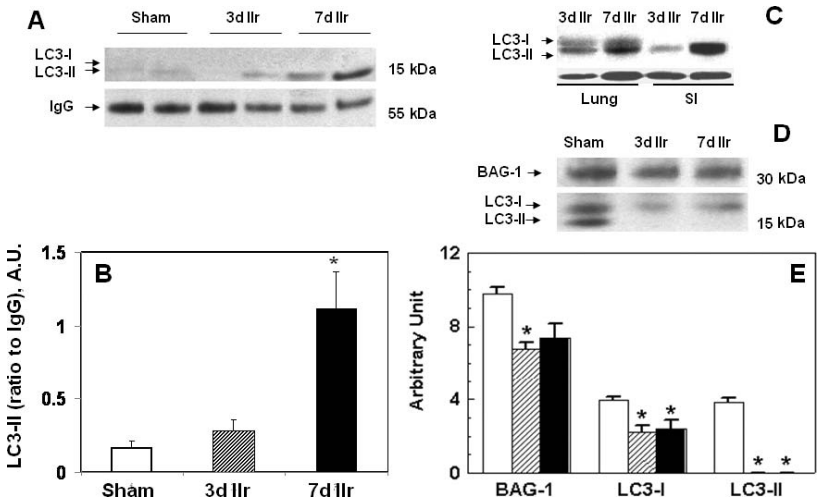

Figure 3. Effect of ionizing irradiation on LC3 status in small intestine tissue of CD2F1 mice. Representative western blot of the LC3-I and LC3-II proteins (A) and densitometrical analysis of the bands of the LC3-II protein (B); $^{*}p < 0.05$ vs. sham treatment, days 3 and 7 following ionizing irradiation, $n = 5$; determined by one-way ANOVA with Tukey *post hoc* correction. (C) Comparison of profiles of blotting bands of LC3-I and LC3-II isoforms expressed in lung and small intestinal tissue from irradiated mice. Assessment of alterations of interaction of both LC3 and BAG-1 with HSP-70 was conducted using co-immunoprecepitation of the LC3 and BAG-1 proteins with HSP-70 protein. The results are presented in (D) (western blot) and (E) (densitometry histograms); open bars, sham treatments; hatched bars, day 3 post-irradiation animal group; solid bars, day 7 post-irradiation animal group. $^{*}p < 0.05$ versus sham treatment, $n = 3$; determined by Student's *t*-test

its actions (including suppression of apoptosis) via binding HSP-70 and Bcl-2 proteins [30,31]. Expression of HSP-70 has been shown recently to suppress LC3-dependent vacuolization *in vitro* [32]. Small intestine tissue lysates obtained from sham-treated and ionizing irradiation-treated animals were immunoprecipitated with HSP-70 specific antibody and the immunoprecipitates were analysed for autophagosomal membrane proteins LC3-II and BAG-1 by Western immunoblotting. The results of analysis of co-precipitation of LC3 with HSP-70 (Figure 3D, E) showed that irradiated small intestine had a lower

amount of LC3 capable of interacting with HSP-70 (compared to sham treatment). This effect could result in a decrease in HSP-70-dependent inhibition of LC3-dependent vacuolization in irradiated small intestine. We found a small significant reduction in BAG-1 co-precipitation with HSP-70 between ionizing irradiation and sham-treated specimens (Figure 3D, E).

The ionizing irradiation-associated up-regulation of the autophagy pathway determined by immunochemical analysis of LC3 protein was confirmed using confocal immunofluorescence imaging of LC3 protein in small intestine specimens. The projections of LC3 protein in the specimens and relative intensity of immunofluorescence of LC3 are shown in Figure 4. The intensity of LC3 immunofluorescence was significantly higher after ionizing irradiation treatment, with its prevalent expression at the region of the small intestinal crypt (Figure 4B, D) as compared to that in sham-treated tissue (Figure 4A, C). The increase in the LC3 immunofluorescence was accompanied by the appearance of LC3-abundant vesicular formations in the crypt cells (Figure 4B, inset), which were further identified as Paneth cells by their pyramidal shape and immunoreactivity for CD15 receptors (Figure 5). The formation of multilayer vesicular structures in these high-granularity cells was visualized using TEM

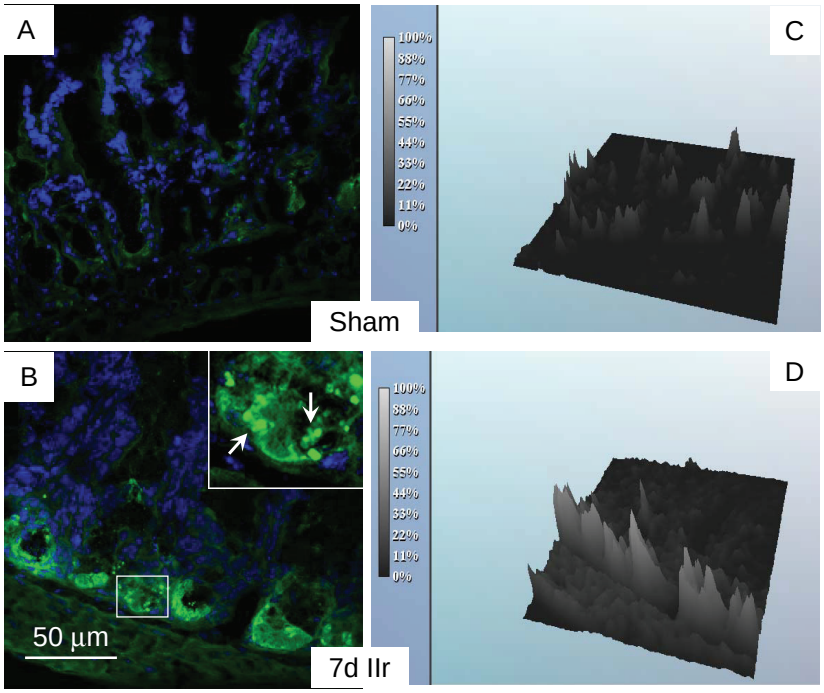

Figure 4. Immunofluorescence confocal imaging of the LC3 protein in small intestine. (A, B) Representative projections revealing LC3 protein (green channel) in small intestinal specimens obtained from a sham-treated animal and an irradiated animal, respectively. (C, D) Assessment of relative immunofluorescence of the LC3 protein in the projections presented in (A) and (B), respectively. Counterstaining of nuclei with Hoechst 33342 appears in blue. The confocal images were taken with a pinhole set-up to obtain 0.5 µm Z-sections

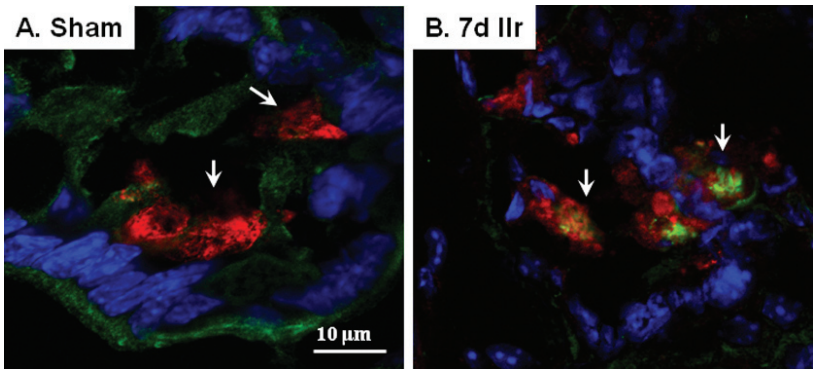

Figure 5. Assessment of LC3 immunoreactivity in the CD15-positive (Paneth) crypt cells. (A) Projections revealing CD15 (red channel) and LC3 (green channel) in a sham-treated specimen. (B) Same as (A) except that the image represents alterations at day 7 following ionizing irradiation. Co-localization of CD15 and LC3 is shown in yellow as result of interference of green and red colours (B). CD15-positive cells are indicated by arrows. Vacuole vesicles with 200–900 nm diameters were identified as autophagosomes. The confocal images were taken with pinhole set-up to obtain 0.5 µm Z-sections. (A, B) Representative images of analyses conducted using five specimens in each group

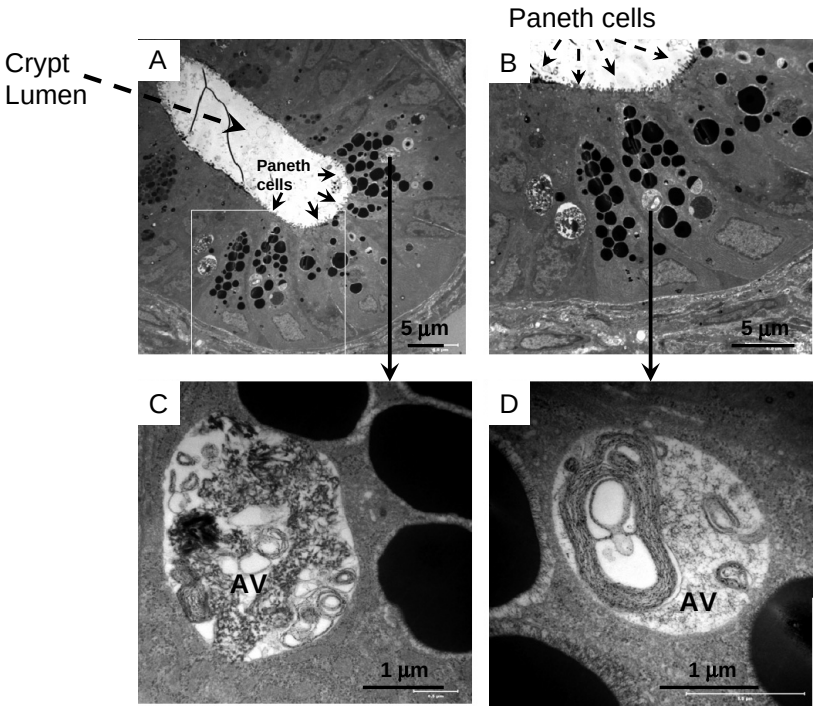

Figure 6. Electron micrographs of autophagic vacuoles (AV) observed at the bottom of the small intestine crypts in the high-granularity pyramid-shaped Paneth cells of irradiated small intestine. (A) Low magnification image of small intestinal crypt. The pyramid-shaped Paneth cells are observed at the bottom of the crypt and are indicated by arrows in (A, B). (B) High magnification image of the white rectangular box indicated in (A). (C–D) Micrographs of multilamellar AV in Paneth cells

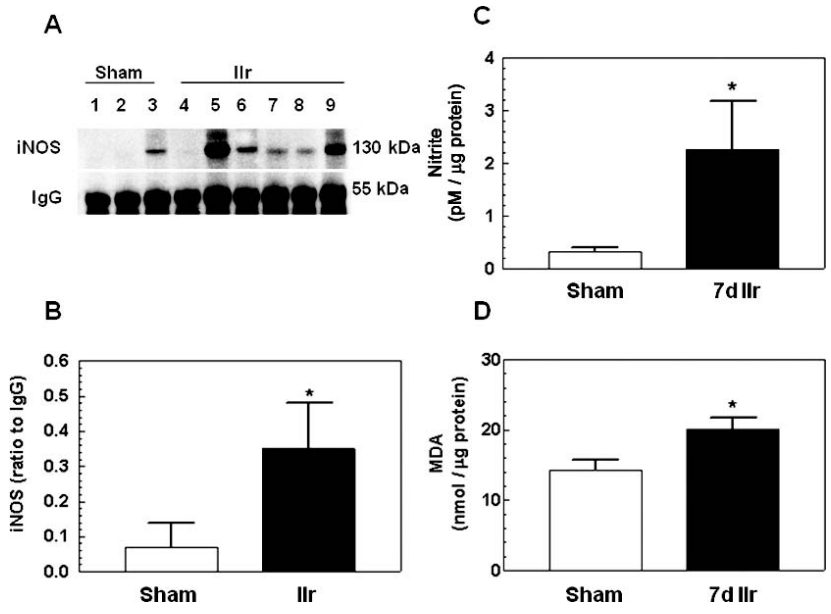

Figure 7. Gamma irradiation increases iNOS protein, NO production and lipid peroxidation in mouse jejunum. After γ-irradiation at 9.25 Gy, the ileum collected at 4 h post-ionizing irradiation was analysed for the level of its iNOS protein. (A) Representative gels of iNOS protein and IgG are presented. (B) The band of iNOS protein was quantified densitometrically and normalized to IgG. The ileum collected at day 7 following ionizing irradiation was lysed and its lysates were assayed for NO production (C) and lipid peroxidation (D). $^*p < 0.05$ vs. sham group, $n = 3$; determined by Student's *t*-test

techniques (Figure 6). These structures were similar to those shown recently by other authors and identified as autophagosomes [18,33].

Assessment of nitrative and oxidative stress in small intestine

Oxidative modification of Atg4 is considered to be a non-specific mechanism of stress-induced autophagy [11,12]. A crucial role of oxidative protein nitration and iNOS-dependent formation of 3NTyr in cell signalling is well documented [34]. The overall results on activation of the iNOS pathway in the small intestine after ionizing irradiation are shown in Figure 7. Ionizing irradiation was followed by a 5.7-fold increase in iNOS protein (Figure 7A, B) that was accompanied by both a 10-fold increase in

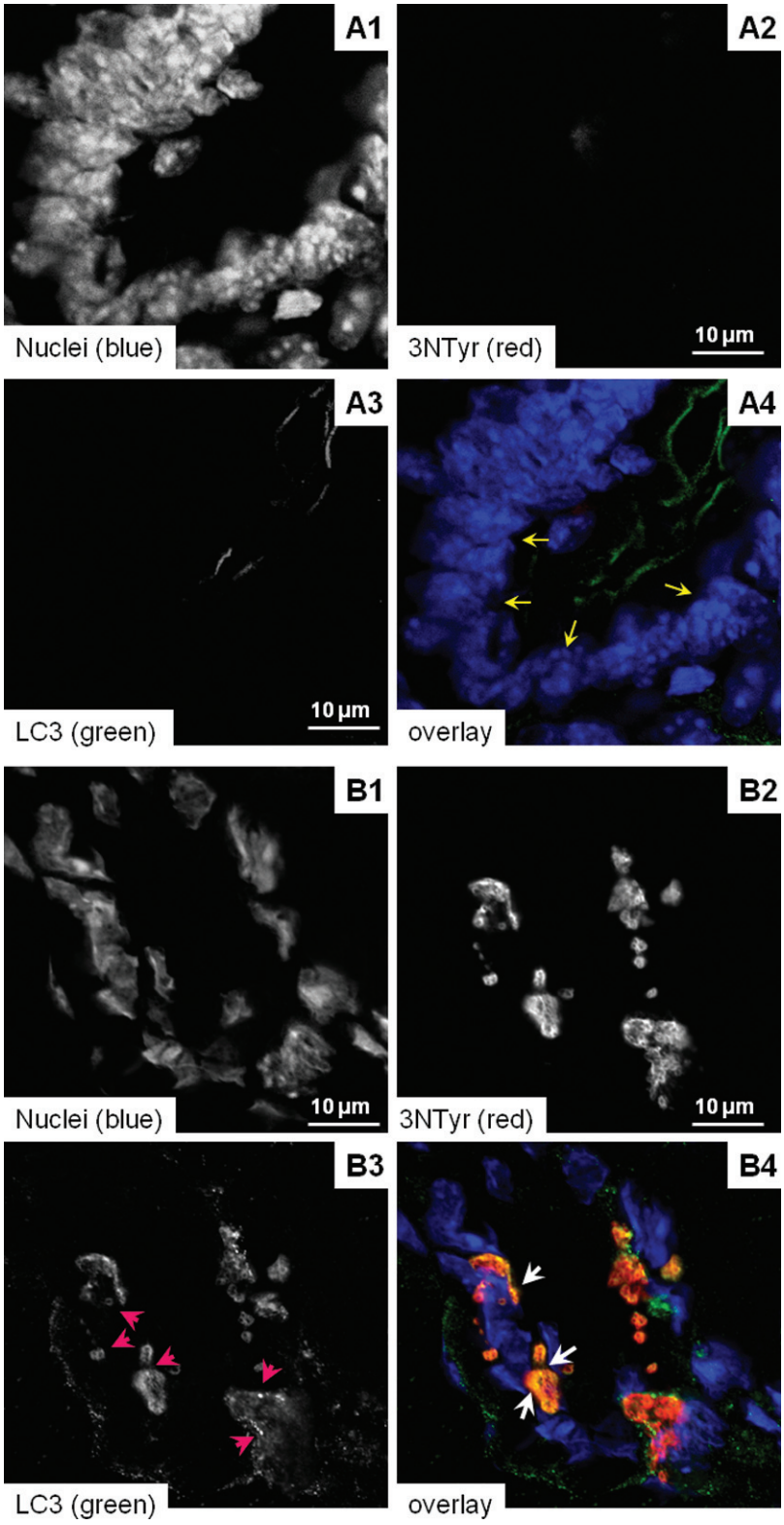

Figure 8. Confocal imaging of immunoreactivity of nitrated proteins (3NTyr) and the LC3 protein in the small intestine crypt cells. (A1–A4) Projections of 3NTyr (red channel, A2), LC3 (green channel, A3), nuclei (blue channel, A1), and overlay of all the above (A4) obtained from a specimen of sham-treated small intestine. (B1–B4) Projections of 3NTyr (red channel, B1), LC3 (green channel, B3), nuclei (blue channel, B1) and overlay of all the above (B4) obtained from a small intestine specimen collected at day 7 following ionizing irradiation. Formation of autophagy vacuoles is indicated by red arrows in the green channel (LC3) image. Spatial co-localization of 3NTyr and LC3 is shown in yellow as a result of interference of green and red colours, and is indicated by white arrows. The confocal images were taken with a pinhole set-up to obtain 0.5 µm Z-sections. Sets (A) and (B) are representative images of analyses conducted using five specimens in each group

nitrites and accumulation of MDA in the specimens (Figure 7C, D).

The results of confocal imaging are shown in Figure 8A (post-sham treatment) and Figure 8B

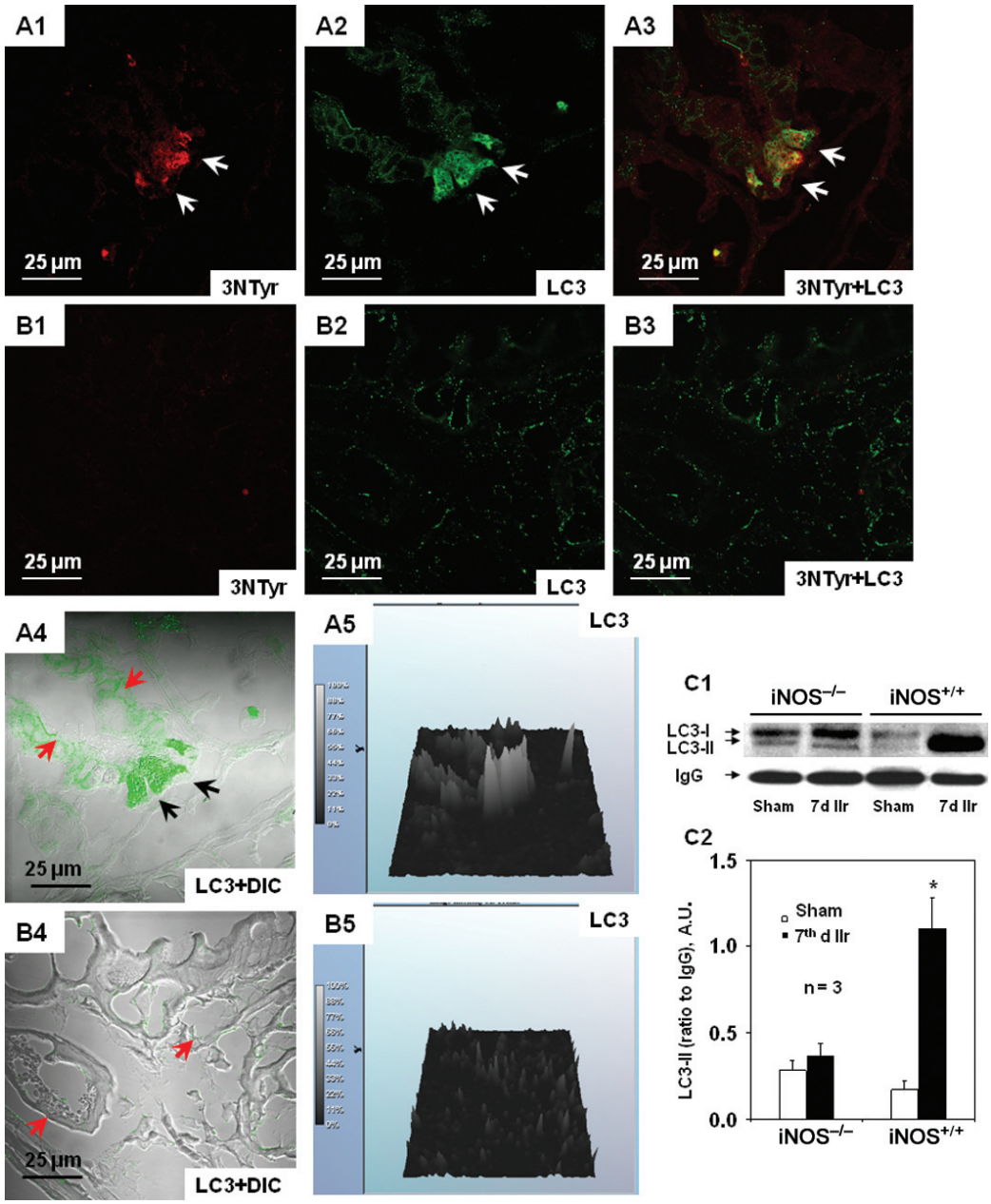

Figure 9. Comparison of immunoreactivity for nitrated proteins (3NTyr) and the LC3 protein in the small intestinal crypt cells of iNOS knockout (B6.129P2-*NOS2*^{tm1Lau}/J) mice and of wild type CD2F1 mice at day 7 following irradiation. (A1–A5) Images obtained from small intestine specimens of CD2F1 mice. (B1–B5) Images obtained from small intestine specimens of B6.129P2-*NOS2*^{tm1Lau}/J mice. Projections for 3NTyr are presented in (A1, B1). Projections for LC3 are presented in (A2, B2). Superposition of projections for 3NTyr and LC3 is presented in (A3, B3). Morphological localization of LC3 immunoreactivity in small intestine specimens is determined using superposition of SI DIC images and respective LC3 immunofluorescence images (A4, B4). Histograms of relative immunofluorescence of LC3 in the small intestine specimens are shown in (A5, B5). Relatively lower levels of the immunoreactivity of 3NTyr and LC3 protein was observed in small intestine specimens of B6.129P2-*NOS2*^{tm1Lau}/J mice as compared to those of CD2F1 mice. The confocal images were taken with pinhole set-up to obtain 0.5 µm Z-sections. (C1) Immunoblot assessment of LC3-II protein in the irradiated small intestine of B6.129P2-*NOS2*^{tm1Lau}/J and CD2F1 mice. (C2) Respective densitometry of LC3-II bands presented in (C2). $^{*}p < 0.05$ versus irradiated B6.129P2-*NOS2*^{tm1Lau}/J group, $n = 3$; determined by Student's *t*-test

(post-ionizing irradiation). The specimens obtained from irradiated animals manifested a substantial increase in 3NTyr immunofluorescence (Figure 8B2) that was mainly observed in the lower part of the crypt region and had high spatial correlation ($r = 0.79$) with immunofluorescence of the LC3 protein (Figure 8B3). A combined assessment of immunoreactivity of LC3, 3NTyr and CD15 has confirmed a substantial increase in the expression of LC3 protein in Paneth cells affected by 3NTyr formation (not shown). Given these findings, we further attempted to prove the presence of interplay of the activated pro-oxidative iNOS pathway with the mAG pathway. With this goal, we compared the immunoreactivity of LC3 and 3NTyr in the small intestine crypt cells of both CD2F1 and iNOS knockout B6.129P2-*NOS2*^{tm1Lau}/J mice and

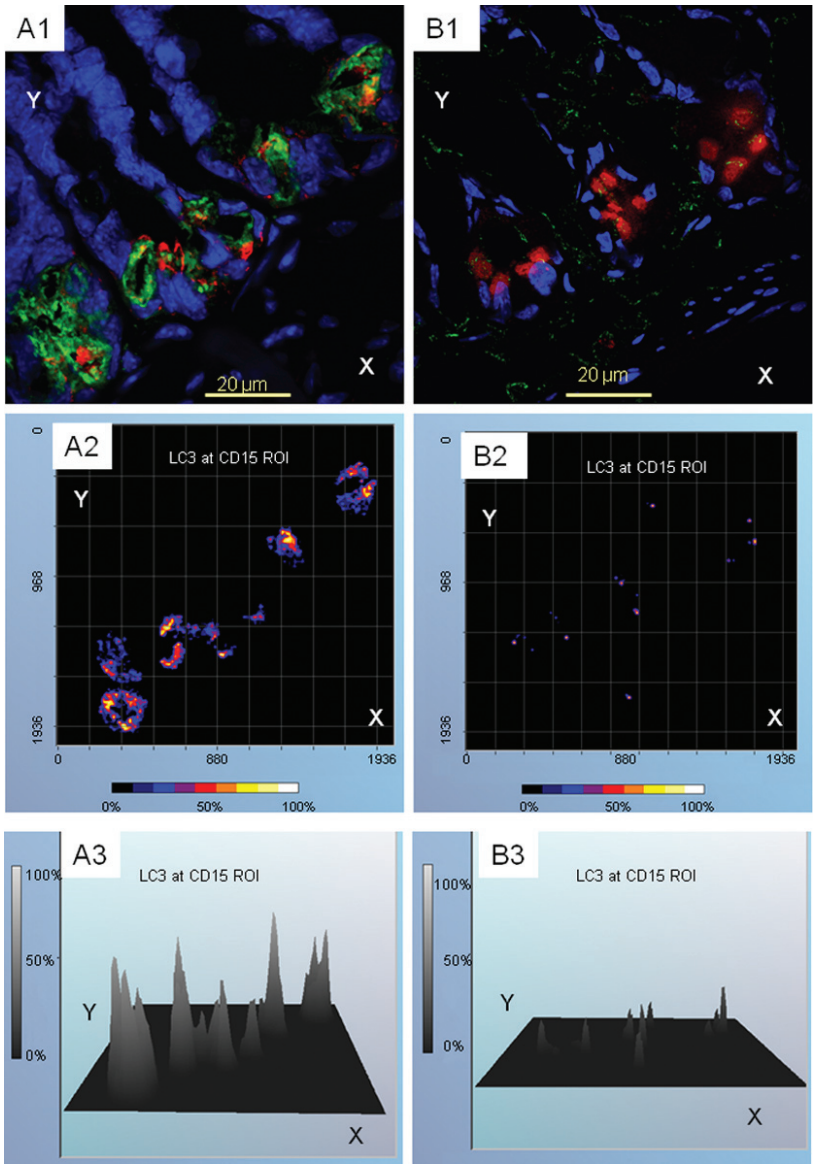

Figure 10. Confocal image analysis of immunoreactivity of the LC3 protein in the CD15-positive crypt Paneth cells of CD2F1 mice (A) and iNOS knockout (B6.129P2-*NOS2*^{tm1Lau}/J) mice (B) at day 7 following irradiation. Superpositions of projections of LC3 (green channel) and CD15 (red channel) in 0.5 µm Z-sections are presented in (A1; CD2F1 mice) and (B1; B6.129P2-*NOS2*^{tm1Lau}/J mice). The blue channel shows counterstaining of the nuclei with Hoechst 33 342. ROI analysis of two-dimensional spatial co-localization of LC3 immunofluorescence and CD15 immunofluorescence, obtained from (A1) and (B1), is presented in (A2) and (B2), respectively, and immunofluorescence intensity in (A3) and (B3)

correlated the effect with levels of oxidative stress in small intestine tissue.

The analyses demonstrated that, in contrast to CD2F1 mice, irradiation of B6.129P2-*NOS2*^{tm1Lau}/J mice did not cause a statistically significant increase in NO production (in pM/µg protein, sham: 1.54 ± 0.22 versus ionizing irradiation: 2.23 ± 0.53, $p > 0.05$, Student's t-test) or MDA (in nM/µg protein, sham: 1.30 ± 0.13 versus ionizing irradiation: 1.12 ± 0.32, $p > 0.05$, Student's t-test) in small intestine tissue. In concord with these data, 3NTyr formation and the LC3-II level in small intestine specimens of irradiated B6.129P2-*NOS2*^{tm1Lau}/J mice were significantly lower than those observed in irradiated CD2F1 mice. The discrepancy in the LC3 immunoreactivity between these two types of mouse was shown with confocal imaging (Figure 9A, B) and confirmed by immunoblot analysis of the LC3-II isoform (Figure 9C). The status of LC3 in Paneth cells in the two groups of irradiated mice was assessed with region of interest (ROI) analysis of CD15-associated LC3 immunofluorescence. As shown in Figure 10, the level of LC3 protein was substantially higher (~10-fold) in Paneth cells of CD2F1 mice compared to B6.129P2-*NOS2*^{tm1Lau}/J mice. One caveat of the approach used is that the iNOS-deficient mice are on a different genetic background than mice with wild-type iNOS function, and this leaves open a possibility of other mechanisms (aside from iNOS activity) contributing to the observed effect in the B6.129P2-*NOS2*^{tm1Lau}/J phenotype.

Discussion

We have shown that a high dose of γ-ionizing irradiation (9.25 Gy) up-regulates LC3-II (an autophagosome-specific protein) and formation of mAG vacuoles (AVs) in mouse small intestine at day 7 following ionizing irradiation (Figure 3). Spatial image analysis reveals a high level of mAG events in Paneth cells at the crypts of Lieberkühn, where Paneth cells were identified morphologically and by positive immunostaining for CD15 (Figures 4–6, 8, 9). We assume that up-regulation of this pathway in Paneth cells can be a part of response to the damage produced by ionizing irradiation to crypt cells and can be associated with the activation of pro-oxidant metabolic pathways. This assumption connects the presented observations with the concept of a crucial role of mAG in cell reconstitution and survival [4–7,11,12,35]. This interpretation of the data does not exclude other mechanisms, such as an increase in the secretory activity of Paneth cells in irradiated small intestine as part of the compensatory response of the innate defence system to the ionizing irradiation-induced damage to leukocyte tissue. The latter is in concord with a concept by Cadwell and co-authors of a key role of mAG in the granule exocytosis pathway in Paneth cells [36,37]. Taken together, activation of mAG following ionizing irradiation can be important for crypt homeostasis.

Up-regulation of mAG under redox-stress conditions can occur at transcriptional, post-transcriptional and post-translational levels. A range of processes are involved, including expression of Atg genes mediated by redox-signalling mechanisms, unfolding of constitutively expressed mRNAs bound to redox-sensitive mRNA-binding proteins, unfolding of autophagy proteins (Atgs) bound by stress-sensitive chaperones, and redox-dependent enzymatically-controlled conversion of autophagy proteins (as proposed recently for LC3-I) [16,17,38,39].

Here we assessed the dynamics of LC3 protein to track mAG in small intestine cells in the post-irradiation period. The observed increase in the levels of LC3-II in the irradiated small intestine were unlikely due to transactivation of the *Atg8* gene, since we did not find a significant difference in *Atg8* mRNA levels between irradiated and sham groups (Gorbunov and Kiang, unpublished data). However, the presence of high levels of constitutive *Atg8* mRNA in the analysed specimens might suggest the involvement of post-transcriptional and post-translational mechanisms in the production of LC3-II. One of the explanations for the mAG effect in the presented model is iNOS/NO-dependent post-transcriptional expression of LC3-I, followed by redox-dependent conversion of LC3-I to LC3-II mediated by Atg4 [9,22,38,39]. Indeed, NO can orchestrate post-transcriptional gene regulation by modulation interactions between RNA-binding proteins and regulatory elements in the untranslated regions of mRNA, which in turn can modulate mRNA stability and translational efficiency and ultimately lead to accumulation of LC3 protein [39,40]. In this report, LC3-II immunoreactivity was observed in the irradiated CD2F1 ($iNOS^{+/+}$) mice and was preceded by activation of the iNOS pathway (Figures 9, 10). At day 7 following ionizing irradiation, protein nitration occurred in crypt Paneth cells of CD2F1 ($iNOS^{+/+}$) mice, where the immunoreactivity of 3NTyr co-localized with the immunoreactivity of LC3 and AV (Figure 9). The observed effects were diminished in iNOS knockout B6.129P2-*NOS2*^{tm1Lau}/J mice subjected to the same treatments. Taken together, alterations in the cell redox status could trigger the Atg4-dependent conversion of LC3-I to LC3-II and thus stimulate autophagy at the site of oxidation. However, we cannot exclude other mechanisms for activation of LC3-II pathway in the irradiated animals.

Analysis of literature data suggests that an important step in mAG activation can be the release of LC3-I and LC3-II proteins folded by HSP-70 in conjunction with its activator and co-chaperone BAG-1 to further promote vacuolization [32,41,42]. Herein, we showed that up-regulation of autophagy was accompanied by decrease in protein–protein interaction between LC3, HSP-70 and BAG-1 that was consistent with the discussed literature data.

In summary, ionizing irradiation increased LC3-II in CD15-positive Paneth cells at day 7 following exposure. The increase was correlated with iNOS activation, NO production, lipid peroxidation and protein nitration. Whether mAG is specifically up-regulated by iNOS signalling mechanism, or interferes with other pathways, such as innate antibacterial response, in irradiated small intestine, is not known and requires further investigation.

Acknowledgements

The authors thank Dr Dennis P. McDaniel for his help with TEM analysis and Ms Joan Smith, Ms Sarah Leggate, Mr Rex Hartzorger and Mr Bradley Garrison for their technical support. This study was supported by Armed Forces Radiobiology Research Institute (AFRRI) Intramural Grant No. RAB2CF (to JGK) and the National Institute of Allergy and Infectious Diseases (NIAID), Grant No. YI-AI-5045-04 (to JGK).

References

1. Potten CS, Merritt A, Hickman J, Hall PA, Faranda A. Characterization of radiation-induced apoptosis in the small intestine and its biological implications. *Int J Radiat Biol* 1994;**65:**71–78.
2. Coopersmith CM, Gordon JI. γ-Ray-induced apoptosis in transgenic mice with proliferative abnormalities in their intestinal epithelium: re-entry of villus enterocytes into the cell cycle does not affect their radioresistance but enhances the radiosensitivity of the crypt by inducing p53. *Oncogene* 1997;**15:**131–141.
3. Verheij M, Bartelink H. Radiation-induced apoptosis. *Cell Tissue Res* 2000;**301:**133–142.
4. Rumio C, Besusso D, Palazzo M, Selleri S, Sfondrini L, Dubini F, *et al*. Degranulation of Paneth cells via toll-like receptor 9. *Am J Pathol* 2004;**165:**373–381.
5. Mathan M, Hughes J, Whitehead R. The morphogenesis of the human Paneth cell. An immunocytochemical ultrastructural study. *Histochemistry* 1987;**87:**91–96.

6. Porter EM, Bevins CL, Ghosh D, Ganz T. The multifaceted Paneth cell. *Cell Mol Life Sci* 2002;**59:**156–170.
7. Ouellette AJ, Hsieh MM, Nosek MT, Cano-Gauci DF, Huttner KM, Buick RN, *et al*. Mouse Paneth cell defensins: primary structures and antibacterial activities of numerous cryptidin isoforms. *Infect Immun* 1994;**62:**5040–5047.
8. Hampton JC. Effects of ionizing radiation on the fine structure of Paneth cells of the mouse. *Radiat Res* 1966;**28:**71–83.
9. Lockshin RA, Zakeri Z. Apoptosis, autophagy, and more. *Int J Biochem Cell Biol* 2004;**36:**2405–2419.
10. Terman A, Brunk UT. Autophagy in cardiac myocyte homeostasis, aging, and pathology. *Cardiovasc Res* 2005;**68:**355–365.
11. Kundu M., Thompson CB. Autophagy: basic principles and relevance to disease. *Annu Rev Pathol* 2008;**3:**247–255.
12. Schmid D, Münz C. Innate and adaptive immunity through autophagy. *Immunity* 2007;**27:**11–21.
13. Fengsrud M, Sneve ML, Overbye A, Seglen PO. Structural aspects of mammalian autophagy. In *Autophagy*, Klionsky DJ (ed.). TX' Landes Bioscience: Georgetown, TX, 2004; 11–25.
14. Levine B, Klionsky DJ. Development by self-digestion: molecular mechanisms and biological functions of autophagy. *Dev Cell* 2004;**6:**463–477.
15. Ohsumi Y. Molecular dissection of autophagy: two ubiquitin-like systems. *Nat Rev Mol Cell Biol* 2001;**2:**211–216.
16. Kabeya Y, Mizushima N, Ueno T, Yamamoto A, Kirisako T, Noda T, *et al*. LC3, a mammalian homologue of yeast Apg8p, is localized in autophagosome membranes after processing. *EMBO J* 2000;**19:**5720–5728.
17. Tanida I, Ueno T, Kominami E. LC3 conjugation system in mammalian autophagy. *Int J Biochem Cell Biol* 2004;**36:**2503–2518.
18. Paglin S, Hollister T, Delohery T, Hackett N, McMahill M, Sphicas E, *et al*. A novel response of cancer cells to radiation involves autophagy and formation of acidic vesicles. *Cancer Res* 2001;**61:**439–444.
19. Crighton D, Wilkinson S, O'Prey J, Syed N, Smith P, Harrison PR, *et al*. DRAM, a p53-induced modulator of autophagy, is critical for apoptosis. *Cell* 2006;**126:**121–134.
20. Yorimitsu T, Klionsky DJ. Eating the enoplasmic reticulum: quality control by autophagy. *Trends Cell Biol* 2007;**17:**279–285.
21. Clarke PG. Developmental cell death: morphological diversity and multiple mechanisms. *Anat Embryol (Berl.)* 1990;**181:**195–213.
22. Scarlatti F, Granata R, Meijer AJ, Codogno P. Does autophagy have a license to kill mammalian cells? *Cell Death Differ* 2009;**16:**12–20.
23. Institute for Laboratory Animal Research. *Guide for the Care and Use of Laboratory Animals*. National Academy Press, Washington, D.C. 1996.
24. Withers HR, Elkind MM. Radiosensitivity and fractionation response of crypt cells of mouse jejunum. *Radiat Res* 1969;**38:**598–613.
25. Garabedian EM, Roberts LJ, McNevin MS, Gordon JI. Examining the role of Paneth cells in the small intestine by lineage ablation in transgenic mice. *J Biol Chem* 1997;**272:**23729–23740.
26. Potten CS, Owen G, Booth D. Intestinal stem cells protect their genome by selective segregation of template DNA strands. *J Cell Sci* 2002;**115:**2381–2388.
27. Barker N, van Es JH, Kuipers J, Kujala P, van den Born M, Cozijnsen M, *et al*. Identification of stem cells in small intestine and colon by marker gene *Lgr5*. *Nature* 2007;**449:**1003–1007.
28. Atkins JL, Hammamieh R, Jett M, Gorbunov NV, Asher LV, Kiang JG. α-Defensin-like product and asymmetric dimethylarginine increase in mesenteric lymph after hemorrhage in anesthetized rat. *Shock* 2008;**30:**411–416.
29. Gorbunov NV, Das DK, Goswami SK, Gurusamy N, Atkins JL. Spatial coordination of cell adhesion molecules and redox cycling of iron in the microvascular inflammatory response to pulmonary injury. *Antioxid Redox Signal* 2007;**9:**483–495.
30. Takayama S, Reed JC. Molecular chaperone targeting and regulation by BAG family proteins. *Nat Cell Biol* 2001;**3:**E237–241.
31. Townsend PA, Stephanou A, Packham G, Latchman DS. BAG-1: a multi-functional prosurvival molecule. *Int J Biochem Cell Biol* 2005;**37:**251–259.
32. Yacoub A, Park MA, Gupta P, Rahmani M, Zhang G, Hamed H, *et al*. Caspase-, cathepsin-, and PERK-dependent regulation of MDA-7/IL-24-induced cell killing in primary human glioma cells. *Mol Cancer Ther* 2008;**7:**297–313.
33. Yan L, Vatner DE, Kim SJ, Ge H, Masurekar M, Massover WH. Autophagy in chronically ischemic myocardium. *Proc Natl Acad Sci USA* 2005;**102:**13807–13812.
34. Rubbo H, Radi R. Protein and lipid nitration: Role in redox signaling and injury. *Biochim Biophys Acta* 2008;**1780:**1318–1324.
35. Ito H, Daido S, Kanzawa T, Kondo S, Kondo Y. Radiation-induced autophagy is associated with LC3 and its inhibition sensitizes malignant glioma cells. *Int J Oncol* 2005;**26:**1401–1410.
36. Cadwell K, Liu JY, Brown SL, Miyoshi H, Loh J, Lennerz JK, *et al*. A key role for autophagy and the autophagy gene *Atg16l1* in mouse and human intestinal Paneth cells. *Nature* 2008;**456:**259–263.
37. Cadwell K, Patel KK, Komatsu M, Virgin HW IV, Stappenbeck TS. A common role for Atg16L1, Atg5 and Atg7 in small intestinal Paneth cells and Crohn disease. *Autophagy* 2009;**5:**250–252.
38. Scherez-Shouval R, Shvets E, Fass E, Shorer H, Gill L, Elazar Z. Reactive oxygen species are essential for autophagy and specifically regulate the activity of Atg4. *EMBO J* 2007;**26:**1749–1760.
39. Mason CA, Chang P, Fallery C, Rabinovitch M. Nitric oxide mediates LC-3-dependent regulation of fibronectin in ductus arteriosus intimal cushion formation. *FASEB J* 1999;**13:**1423–1434.
40. Pantopoulos K, Hentze MW. Nitric oxide signaling to iron-regulatory protein: direct control of ferritin mRNA translation and transferrin receptor mRNA stability in transfected fibroblasts. *Proc Natl Acad Sci USA* 1995;**92:**1267–1271.
41. Stuart JK, Myszka DG, Joss L, Mitchell RS, McDonald SM, Xie Z. Characterization of interactions between the anti-apoptotic protein BAG-1 and Hsc70 molecular chaperones. *J Biol Chem* 1998;**273:**22506–22514.
42. Alberti S, Esser C, Höhfeld J. BAG-1 a nucleotide exchange factor of Hsc70 with multiple cellular functions. *Cell Stress Chaperones* 2003;**8:**225–231.